



Research Article

Sequestration of Pb(II) and Cr(VI) from aqueous environment using low-cost immobilised tannin resin

Bamidele J. Okoli^{1,2}  · Johannes S. Modise^{1,2}

© Springer Nature Switzerland AG 2019

Abstract

The present study was conducted to optimise the process parameters for the extraction of tannin (adsorbent raw material) while minimising waste with the aid of response surface methodology and the application of the immobilised tannin as a mob for metal ions. Based on the reduced second-order polynomial quadratic model, the optimised conditions for the maximum response (tannin): a material mass of 6 g, pH 7, 37.5 °C, 22.5 min and 50 mL of water is required. The immobilised tannin adsorbents; magnetite tannin (MTR) and sulphur doped magnetite tannin resins (S-MTR), were characterised by XRD, FT-IR, TGA, SEM, EDS, BET and an elemental analyser. The influences of pH, contact time, temperature and initial metal ion concentration on adsorption performance of MTR and S-MTR were evaluated. Equilibrium adsorption data were assessed for fitness into four adsorption isotherms and kinetic models. The maximum adsorption capacities of MTR and S-MTR for Pb(II) were observed at optimum pH 4 with adsorption capacities of 534.8 mg/g and 15.1 mg/g, respectively. However, the capacities of MTR and S-MTR for Cr(VI) were 813.0 mg/g, and 709.2 mg/g observed at optimum pH 4 and 2, respectively. Equilibrium data obtained from the uptake of Pb(II) and Cr(VI) ions by MTR and S-MTR best fit into the Langmuir and Freundlich isotherms. Whereas, the sorption of Pb(II) and Cr(VI) on MTR fits into the pseudo-first order while the sorption on S-MTR fits into a pseudo-second-order model. Thermodynamic parameters revealed a feasible, spontaneous and endothermic process for the adsorption of Pb(II) on MTR; however, incorporation of thiourea improves the uptake capacities of both ions from solution but reduces feasibility and spontaneity of the process.

Keywords Adsorption · Cross-linking · Micrograph · Diffractograms · *Acacia* · Thermogravimetric analysis

1 Introduction

Waste management and water quality are one of the two fundamental factors regulating the quality of human health. In the twenty-first century, urbanisation and industrialisation are two major culpable factors that have led to a rapid accumulation of waste and release of heavy metal into our waterways around the world. Heavy metals usually have a large average biological half-life, not readily biodegradable with the propensity of causing secondary

pollution [1, 2], and have severe environmental impacts due to their potential to bio-accumulate causing numerous health disorder [3]. Chromium and lead have been reported as one of the problematic and the leading cause of many health disorders such as skin rashes, haemolysis, renal failure, compromised immune systems, alteration of genetic material, cancer, encephalopathy, vertigo, kidney damage, congenital disabilities, anorexia, liver cirrhosis, hyperthyroidism, and pulmonary fibrosis.

Electronic supplementary material The online version of this article (<https://doi.org/10.1007/s42452-019-0199-8>) contains supplementary material, which is available to authorized users.

✉ Bamidele J. Okoli, okolibj@binghamuni.edu.ng | ¹Institute of Chemical and Biotechnology, Vaal University of Technology, Southern Gauteng Science and Technology Park, Sebokeng, South Africa. ²Department of Chemical Sciences, Faculty of Science and Technology, Bingham University, Karu, Nasarawa State, Nigeria.



SN Applied Sciences (2019) 1:194 | <https://doi.org/10.1007/s42452-019-0199-8>

Received: 4 December 2018 / Accepted: 21 January 2019 / Published online: 31 January 2019

SN Applied Sciences
A SPRINGER NATURE journal

As a result of the increasing health problem caused by the bio- and hyper-accumulations of heavy metals, many technologies have been developed for their removal from the ecological community. Heavy metal pollutants can remove, concentration reduced or oxidation state change by different conventional physico-chemical and biological processes, but the major setback of these treatment techniques is the operational cost while biological treatment is generally less effective and time-consuming [4]. Modern technological techniques currently available for the treatment of wastewater include thermal treatment, desalination, direct reduction, resin adsorption, electrolysis, electrocoagulation, activated carbon adsorption, composite ceramic adsorption, carbon nanofibers adsorption, nanomaterials catalysed reduction, and catalytic reduction [5–7]. Adsorption has been reported as an economical technique for long-term treatment of wastewater [8], which produces a high-quality treated effluent and flexibility in design and operation. One of the commonly applied sorbents is undoubtedly activated carbon. However, production and re-activation of spent carbon are very costly; hence, the urgent need for alternatives [7, 9]. Recently, studies on low-cost sorbent are intensively gaining attention among researchers in the field of wastewater remediation [10]. Studies have shown the rapid increase in the development of low-cost sorbent from various plant sources due to the inability of minerals like Ca^{2+} , Mg^{2+} or alkali metal ions interfere with the chelating of heavy metals as reported by Pradhan et al. [11] in addition to the poly-functional binding site of the sorbent. One of the commonly exploited plant-derived metabolites is the high molecular weight water-soluble polyphenolic tannins sourced from most perennial trees. Tannins bind readily with metals due to the presence of a significant number of adjacent hydroxyl groups in their molecules; although, the solubility of tannins limit their application. However, various techniques have been developed for the immobilisation of tannin before usage [12, 13]. Earlier studies have focused on the sorption capacities of tannin resin from different plants; however, we felt the need to improving the sorption capacities by extending the functionality of tannin sorbents [14, 15].

This paper describes the adsorption behaviour of Pb(II) and Cr(VI) on two modified tannins sorbents and optimisation of five independent extraction parameters of raw tannin by response surface methodology.

2 Experimental

2.1 Reagents

Analytical grade ammonia solution, benzaldehyde, sodium hydroxide, hydrochloric acid, nitric acid, lead nitrate ($\text{Pb}(\text{NO}_3)_2$), potassium dichromate ($\text{K}_2\text{Cr}_2\text{O}_7$), ferric chloride

hexahydrate ($\text{FeCl}_3 \cdot 6\text{H}_2\text{O}$), ferrous sulphate heptahydrate ($\text{FeSO}_4 \cdot 7\text{H}_2\text{O}$), and thiourea were purchased from Sigma Aldrich, USA.

2.2 Optimisation of tannin extraction conditions

Five essential parameters were optimised using the Box-Behnken response surface model involving forty-three experimental runs in three replicates to maximise the yield of tannin [16, 17]. The five design variables were the mass of stem bark (X_1), contact time (X_2), temperature (X_3), solvent volume (X_4), and pH (X_5) (Table 1).

At the end of the quantitative studies, the data were fitted into a second-order polynomial Eq. (1) generated by the response surface model:

$$Y = \beta_0 + \sum_{i=1}^5 \beta_i X_i + \sum_{i=1}^5 \beta_{ii} X_i^2 + \sum_{i < j=1}^5 \beta_{ij} X_i X_j \quad (1)$$

where Y is the predicted tannin yield (mg TAE/g), while β_0 , β_i , β_{ii} , and β_{ij} are the regression coefficients for intercept, linear, quadratic and interaction terms, respectively, X_i and X_j are the independent variables. To evaluate the adequacy of the model, the Fisher test value (F-value), coefficient of regression (R^2) and the lack of fit obtained from the analysis of variance (ANOVA) at $P < 0.05$ were evaluated. The effects of unexplained variability in the observed response due to extraneous factors were minimized by randomising the order of experiments. 3D response surface plots were also generated by keeping one response variable at its optimal level and plotting it against four independent variables.

2.3 Synthesis of tannin-resin

The optimized extracted tannin was vacuum filtered, freeze-dried at -55°C , and finally, the dark brown *A. decurrens* tannin powder was collected. To 300 g of the tannin powder an equimolar solution of ammonia and benzaldehyde was mixed at 1500 rpm for 5 min. The mixture was

Table 1 Independent variables and their coded and actual values used for optimisation

Independent variable	Units	Symbol	Coded levels		
			-1	0	1
Mass of stem bark	G	X_1	3.0	4.5	6.0
Contact time	Rpm	X_2	15.0	22.5	30.0
Temperature	Hr	X_3	25.0	37.5	50.0
Solvent volume	mL	X_4	50.0	75.0	100.0
pH		X_5	4.0	7.0	10.0

suction-filtered and the residue collected. Afterward, the residue was immersed in 0.9 L deionised water, warmed for 3 h at 70 °C; and suction filtered again. The obtained residue was heated for 30 min in a solution of 0.1M HNO_3 . Subsequently, the insoluble mixture was kept at 80 °C, dried, pulverised and sieved to 100 μm particle sizes.

2.4 Synthesis of magnetite and sulphur doped magnetite

To 80 mL of degassed deionised water, 3.1 g of $\text{FeCl}_3 \cdot 6\text{H}_2\text{O}$ and 2.1 g of $\text{FeSO}_4 \cdot 7\text{H}_2\text{O}$ were introduced and agitated at 550 rpm for 10 min, followed by the addition of 40 mL of 25% aq. NH_3 . After 5 min, 20 g of tannin-resin powder was introduced and stirring for a further 60 min, after which the reactor was dismantled, and the magnetite tannin-resin (MTR) harvested. The MTR was generously washed with deionised H_2O to a pH 7.0; after that, freeze-dried to obtain a dark powdered material [18] (Fig. 1).

Dried MTR powdered (9.0 g) was doped for 15 h with 0.02 g/mL of thiourea solution pre-heated at 25 °C. The mixture was further heated at 80 °C to almost dryness, washed severally to remove any unreacted thiourea and

freeze-dried under vacuum at -55 °C and 215 mTorr for 48 h to obtain S-MTR. The dried MTR and S-MTR were then pulverised and sieved to 100 μm particle sizes and stored in an airtight container for further use.

2.5 Preparation of stock solution

Stock solutions of Pb(II) and Cr(VI) were prepared by dissolving 1.5980 g ($\text{Pb}(\text{NO}_3)_2$) and 2.835 g $\text{K}_2\text{Cr}_2\text{O}_7$ in 1 L of water from Vaal river (29°4'15"S 23°38'10"E), South Africa to stimulate an environmental condition. Series of 100 mL conical flasks containing Pb(II) and Cr(VI) ions at predetermined concentrations were prepared.

2.6 Characterisations

The following instruments were used for the characterisation of the adsorbents; thermogravimetric analyser (TGA) (Perkin Elmer, Waltham, MA), FT-IR (PerkinElmer Spectrum 400, Waltham, MA), X-Ray Diffractometer (XRD) (ZEISS Sigma 300, Oberkochen, Germany), scanning electron microscope (SEM) (JSM-7500F, Tokyo, Japan), Brunauer–Emmett–Teller analyser (BET) (Nova 3200e,

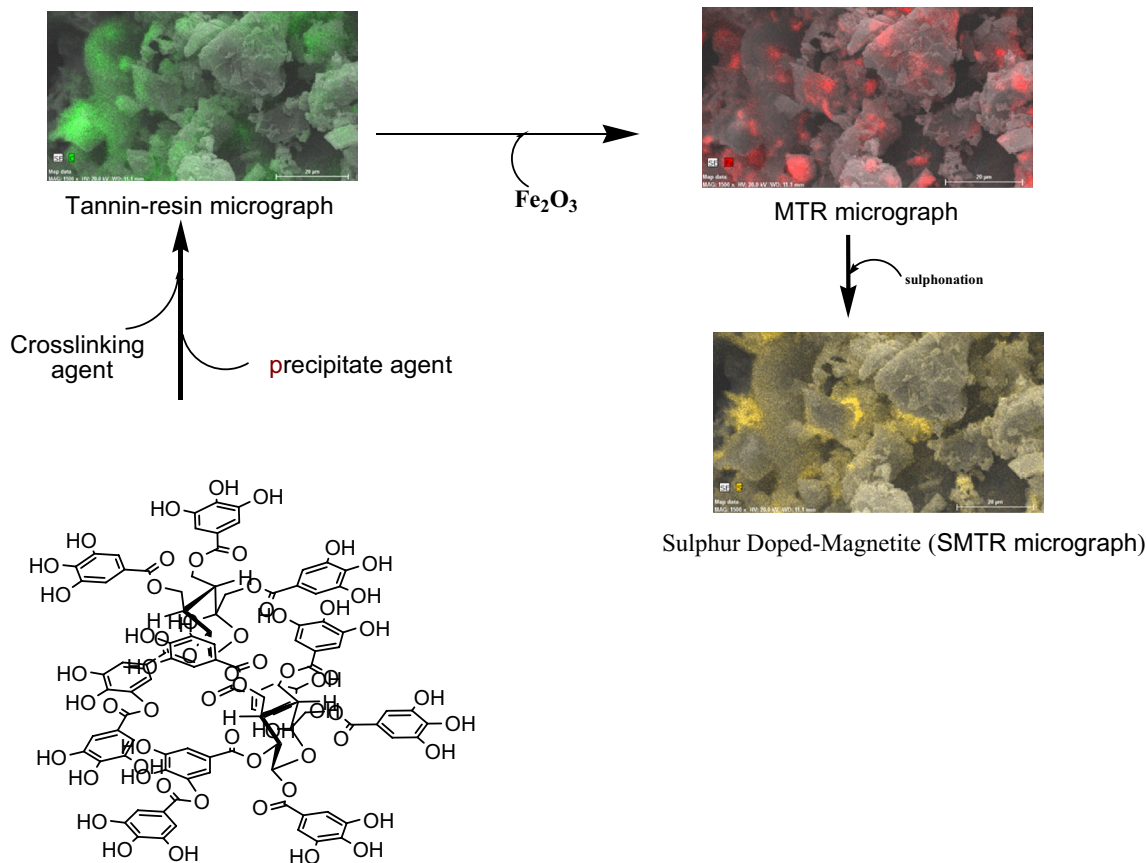


Fig. 1 Graphical synthetic route of MTR and S-MTR

Boynton Beach, FL), energy-dispersive X-ray spectroscope (EDS) (Analytical, Tokyo, Japan), and the metal ion concentrations were determined on an inductively coupled plasma-optical emission spectrometer (ICP-OES) (PerkinElmer, Billerica, MA).

2.7 Batch adsorption study

Based on the parameters under investigation, the pH, contact time or temperature was varied to determine the adsorption capacity of 50 mL of the metal ion solution containing 0.5 g of MTR or S-MTR. At the end of the investigation, the adsorbents were filtered-out, and the final concentration of Pb(II) or Cr(VI) determined using ICP-OES. Thereafter, the amount of metal ion at equilibrium, q_e (mg/g) and at pre-determined time, q_t (mg/g), were estimated according to Eqs. (2), and (3), respectively.

$$q_e = [(C_o - C_e) \times V] / m \quad (2)$$

$$q_t = [(C_o - C_t) \times V] / m \quad (3)$$

where C_o , C_e and C_t (mg/L) are for the initial concentration, equilibrium concentration and the concentration at time t metal ions, respectively. q_e (mg/g) is the adsorbed amount on the sorbate at equilibrium time; V (L) is the volume of the solution; m (g) is the mass of the sorbent.

2.7.1 Effect of pH

The optimum pH for the maximum adsorption efficiency was determined by buffering 50 mL of 100 mg/L metal ion solution within a pH range of 2 to 8 in contact with 0.5 g adsorbent. The desired pH values were achieved by the dropwise addition of 0.1 N HCl or 0.1 N NaOH. The flasks were agitated on a thermostatic-shaker (Selectech, Johannesburg, South Africa) at 150 rpm for 90 min at 25 °C. Afterward, the metal ion concentration was analysed by ICP-OES.

2.7.2 Effect of contact time

The uptake of metal ions by 0.5 g adsorbent at various contact times were studied in a 50 mL metal ion (100 mg/L) solution at the optimised pH. The vials were shaken in a thermostatic shaker at 150 rpm for 5, 10, 15, 20, 25, 30, 40, 50, 60, 70, 80- and 90 min intervals. The metal ion concentrations after filtration were analysed by ICP-OES.

2.7.3 Effect of temperature

Temperature variation (25, 30, 35, 40, 45, 50, 55, 60, 65 and 70 °C) was carried out to investigate the effect of temperature on the adsorption process as well as the enthalpy of

adsorption (ΔH), entropy of adsorption (ΔS) and Gibbs free energy (ΔG) by keeping other parameters constant at 150 rpm for 120 min. 50 mL of 100 ppm of Pb(II) or Cr(VI) aqueous solution was taken in five conical flasks containing 0.5 g of sorbents. The conical flasks were shaken in a thermostatic shaker for equilibrium agitation time. The residual metal ion concentrations after filtration were determined by the use of ICP-OES.

2.7.4 Effect of initial metal ions concentration

The impact of the initial Pb(II) or Cr(VI) concentrations on the adsorption capacity at various concentrations (20, 40, 60, 80, and 100 mg/L) was evaluated at the optimum conditions. At the end of the pre-determined agitation time, the flasks were removed from the shaker and the mixture was filtered through Whatman filter paper. The residual Pb(II) and Cr(VI) concentration were determined by an ICP-OES.

3 Results and discussion

3.1 Optimising the extraction of tannin

The results of the analysis of variance (ANOVA) for response with the corresponding coefficients of multiple determination (R^2) of *A. decurrens* stem bark are presented in the supplementary Table S1. The model was adequate and explains most of the observed variability, while the fitted model, the software generated coefficients, R^2 -values, F-values, and significant probabilities were used to justify the significance of each independent variable.

The maximum theoretical response for tannin (mg TAE/g) was 11.90 mg/TAE/g of stem bark obtained from 43 experimental runs required to determine 20 regression coefficients of the model (Table S1). An excellent fit of the model was generated from the plot of the predicted and actual values ($F = 159.37$; $P = 0.0632$; $R^2 = 0.9329$). The data generated from the response to the five independent variables were transformed into a second-order polynomial Eq. (4); describing the correlation between the independent variables and the amount of tannin:

$$\begin{aligned} \text{Tannin (mg TAE/g)} = & +5.80 + 2.52X_1 + 0.38X_2 + 1.27X_3 \\ & - 2.54X_4 - 0.14X_5 - 0.12X_1X_2 \\ & + 0.13X_1X_3 - 0.075X_1X_4 + 0.22X_1X_5 \\ & - 0.85X_2X_3 - 0.025X_4X_2 \\ & - 1.32X_4X_5 + 0.33X_3X_4 \\ & - 0.12X_3X_5 + 0.58X_4X_5 \\ & - 0.090X_1^2 + 1.24X_2^2 - 0.31X_3^2 \\ & + 0.66X_4^2 + 0.027X_5^2 \end{aligned} \quad (4)$$

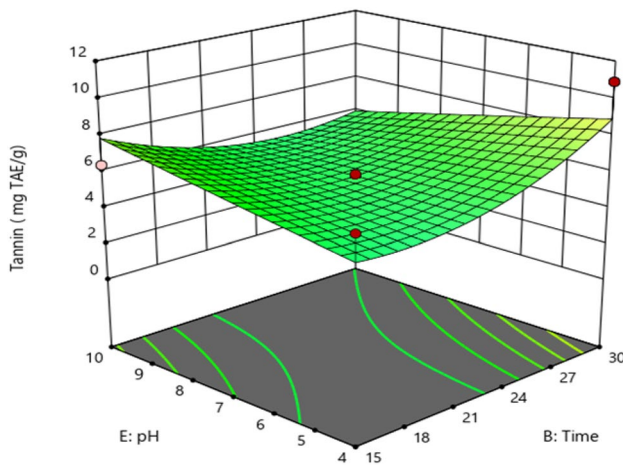


Fig. 2 Graphic surface optimisation for extractable tannin (mg TAE/g) versus (a) X_2 and X_5

The measurement for fitness of the second-order polynomial regression model in Eq. 4 from the adjusted R^2 (0.9893) value, revealed a good degree of correlation between predicted and actual values. Form the analysis of variance result; value of $F=9.17$ confirms a highly significant ($P < 0.0001$) model, that is, there is approximately a 0.01% probability that such large F -value could occur due to noise (Table S1). Also, the lack of fit was insignificant ($P > 0.05$) which implies that the reduced second-order polynomial quadratic model is valid for the spatial influence of the five variables on the amount tannin extracted. The linear terms such as the mass of material, temperature, and volume, the linear interactions between the pH and time (Fig. 2), and the quadratic term of the contact time had statistically significant ($P < 0.05$) effects on the response (tannin mg TAE/g).

The quadratic model revealed that X_4 and X_5 have negative effects on the response, while X_1 , X_2 and X_3 have a

positive impact. The absolute values of X_1 and X_4 are approximately equal and greater than the coefficient of X_2 , X_3 , and X_5 . By implication, the linear terms X_1 and X_4 influence is more significant than those of X_2 , X_3 , and X_5 . The response surface model indicates that the higher the mass of the material at a moderate volume of solvent, the higher the amount of tannin extracted. Based on derivation from the model analysis above, the optimised conditions: a material mass of 6 g, pH 7, 37.5 °C, 22.5 min and 50 mL of water is required for maximum response (tannin).

3.1.1 Verification of results

The suitability of the model equation for predicting the optimum response was further tested using the recommended optimum conditions. There was a close correlation between the experimental and predicted values for each of the responses indicating the development of a satisfactory model (Table 2).

3.2 Characterisation of adsorbents

The percentage compositions of C, H, N, and S in MTR and S-MTR are presented in Table 3. Functionalization of TR with ferrous-ferric and thiourea compounds, caused physicochemical changes in the properties as evident in the 8.47% decrease in the carbon content and a 3.80% increase in sulphur content due to the introduction of Fe^{2+} - Fe^{3+} and organosulfur on the surface of MTR and S-MTR, respectively.

The percentage carbon in the sorbents underline the high carbonaceous characteristic of a high molecular weight tannin from plant materials [19]. The increase in the percentage nitrogen on the sorbents compared to the tannin resin (TR) confirms the successful grafting of nitrogen from precipitating agent unto the surface of the sorbents. Also, the percentage oxygen content of the sorbents

Table 2 Predicted and experimental values of tannin (mg TAE/g) at the optimum conditions

Response	Independent variable				pH	Value	
	Mass (g)	Contact time (min)	Temperature (°C)	Solvent vol. (mL)		Predicted (mg TAE/g)	Experimental (mg TAE/g)
Tannin	6	22.5	37.5	50	7	11.90	10.86 ± 0.52

Table 3 Elemental composition and BET surface area analysis of the sorbent materials

	Elemental composition					Surface area analysis		
	C%	H%	N%	S%	O%	Surface Area (m ² /g)	Pore Volume (cm ³ /g)	Pore Size (nm)
TR	79.00	5.67	5.26	–	10.07	–	–	–
MTR	68.20	5.06	6.26	0.01	20.47	5.5386	0.0330	23.8423
S-MTR	58.40	4.54	6.49	3.81	26.76	1.1810	0.0049	16.4915

equally increased due to the addition of the hydrated iron compounds during magnetite preparation. Similarly, a spike in the percentage sulphur was observed in S-MTR due to the doping of the MTR with thiourea.

The dimensions of the surface area and pore volume of MTR and S-MTR are provided in Table 3. Incorporation of thiourea on MTR to produce S-MTR caused a decrease in the average surface area and total pore volume due to the blockage of internal porosity; hence, the BET surface area and pore volume of S-MTR are smaller compared to MTR.

Isotherm-type classification of the sorbents were determined from the nitrogen adsorption and desorption isotherm plots of the sorbents and are presented in Fig. 3. According to isotherm classification, the adsorbents in this study were observed to generate a typical Type III isotherm [20]; associated with the adsorbate–adsorbate interactions on the surface of the adsorbents. Pore sizes of 16.49–24.84 nm are in the mesopore range which may result in increase in adsorption capacity with increasing surface area; typical of a physisorption process [21, 22].

Interaction of S-MTR with Pb(II) and Cr(VI) ions maybe influenced by a physical process; however, due to the presence of functional binding sites (such as O, S and N) on the sorbents, may result in a predominant chemisorption mechanism.

Thermogravimetric analysis was used to evaluate the thermal stability of TR, MTR and S-MTR and the response presented in Fig. 4. The thermogram of TR showed three steps, initial decomposition occurred at around 36–110 °C with a weight loss of 3.4% which may correspond to the loss of water/moisture. In the contrary, MTR and S-MTR revealed four degradation steps between 30 °C until 200 °C with a total weight loss of about 14%. However,

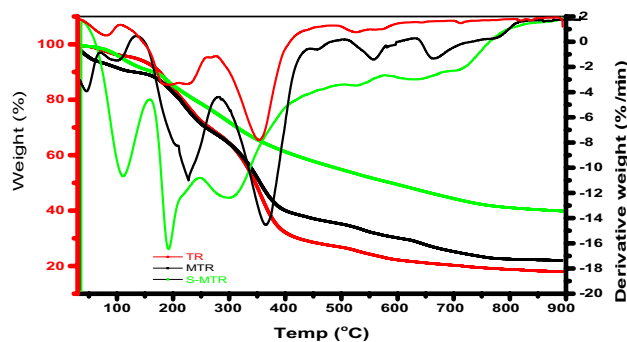


Fig. 4 Thermal response of the TR, MTR and S-MTR

the decomposition observed around 100 °C for TR can be attributed to the loss of chemically bound water in tannin; as observed in MTR and S-MTR due to the affinity of ferrous for oxygenated compounds like water.

The second decomposition stage of TR occurred at 200 °C up to 237 °C with a weight loss of 24.6%. However, the second decomposition stage of MTR and S-MTR showed 21.7% and 13.3% weight loss at a temperature range of 115 °C to 188 °C due to the disintegration of incorporated compounds. At the end of the third stage, there was a total weight loss of 53.5% by TR; whereas, the third decomposition for MTR and S-MTR occurred between 354 °C and 298 °C. The maximum degradation of MTR and S-MTR occurred at temperature 747 °C and 713 °C, respectively with about 49.4% and 27.6% weight loss. Finally, TR generated a total ash content of 46.5% which is lower compared to the 50.6% and 72.4% of MTR and S-MTR due to the incorporation of iron and sulphur

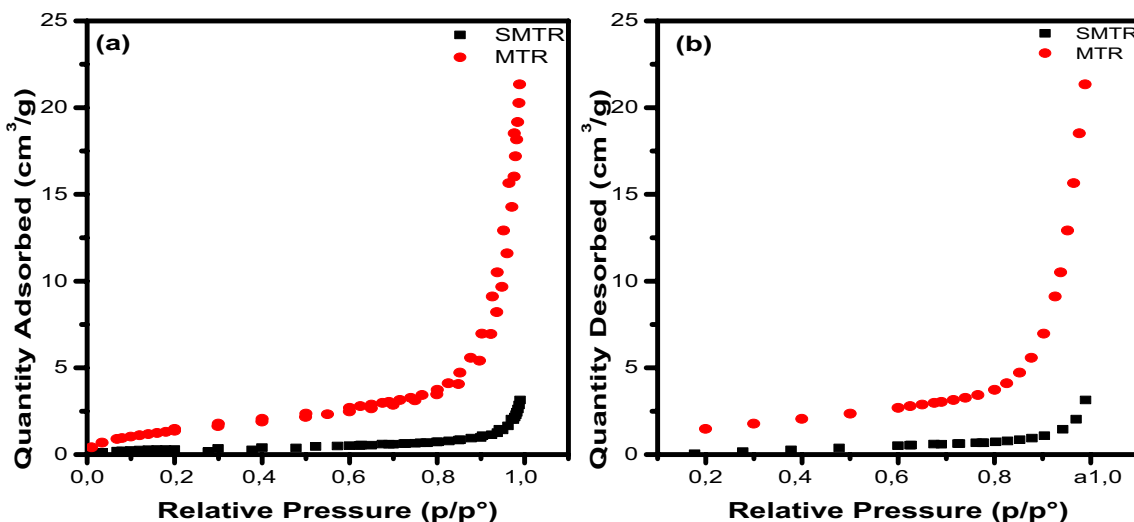


Fig. 3 a Nitrogen adsorption b Nitrogen desorption isotherm plots for S-MTR and MTR

into the sorbents. In conclusion, the thermal stability of the sorbents was raised from 273.7 °C to around 747 °C.

XRD patterns of the sorbents before and after Pb(II) and Cr(VI) adsorption are shown in Fig. 5. The diffractogram of MTR and S-MTR exhibited several similar diffraction peaks with a slightly different in intensity at the $2\theta = 19.39^\circ$ a characteristic of a semi-crystalline material.

After the uptake of Cr(VI) ion by the adsorbents there was a decrease in the crystalline character; however, an opposite effect was observed when Pb(II) was adsorbed by S-MTR. Therefore, the XRD pattern of S-MTR and MTR after Cr(IV) and Pb(II) adsorption showed broad crystalline peak characteristic of the metal ion.

An N–H stretching vibration was introduced to the sorbents due to the amination reaction during the precipitation of the tannin resin on the spectrum of MTR [23], as well as the peak at 2114 cm^{-1} indicating the presence of thiol in S-MTR [24, 25] (Table 4). However, the appearance of new absorption peaks in the spectrum of S-MTR confirms further the bonding of thiourea functional group to the surface.

The carbonyl C=O and acyl C–O stretch are characteristics of the immobilised tannin material used in the preparation of the sorbents. The absorption peaks of C=O and C=C stretching vibration for aromatic after adsorption of

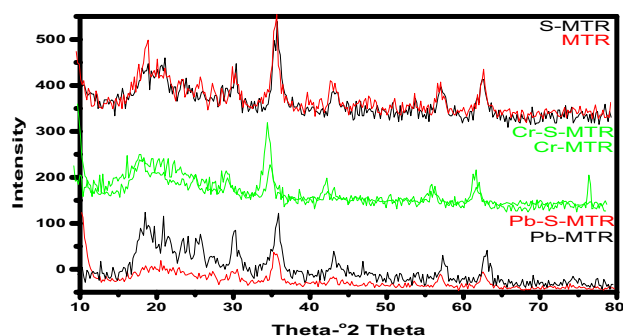


Fig. 5 Diffractogram of the sorbent before and after Pb(II) and Cr(VI) adsorption

metal ions shifted to higher wavenumber. Therefore, the physical and chemical interaction of the metal ions with the sorbents is a confirmation of the changes in absorption peaks position.

Also, the successful crosslinking of the material before the preparation of the sorbents were confirmed by the presence of the C=C stretching and sp^2 C–H bend vibration of the aromatics. The N–H and S–H peaks at 3317 cm^{-1} and 3381 cm^{-1} , respectively were absence after the adsorption; suggesting the involvement of NH and SH groups in Pb(II) and Cr(VI) adsorption.

The micrography of MTR and S-MTR sorbents before and after Pb(II) and Cr(VI) ions adsorption recorded at an accelerating voltage of 3.00 kV, a working distance of 13.0 nm and magnification of 600 X were presented in Fig. 6a–f.

Confirmation of the successful preparation, as well as obtain information on the surface morphology of the sorbents, an SEM imaging technique was employed. Figure 6a showed the surface morphology of MTR with a rough texture, uneven lump, and porous alveolus. Similarly, the surfaces of S-MTR were irregular and porous, with pithy shape cavities after doping of MTR with sulphur; providing an ideal surface for adsorption of metal ions. Figure 6b and c indicated the different surface morphology of MTR sorbent after adsorption. In MTR the adsorption of Pb(II) results in the loss of rough lump while Cr(VI) causes the silver-like fluffy coating on the material (Fig. 6e and c). Changes in the surface morphology after Pb(II) and Cr(VI) adsorption were also observed as the physical appearance of a silver-like coating on the surface; presumably, a monolayer coverage leading to the formation of metal ion-sorbent interaction on the sorbent surface.

Both the EDX spectra (Fig. 7) and colour maps (Fig. 8) recorded at accelerating voltage of 20.0 kV, a working distance of 11.1 nm and magnification of 1.50 K X showed the presence of significant amount carbon in the sorbents. Also, MTR and S-MTR consist of iron (Fe) and sulphur (S) incorporated during the preparation respectively. The Fe

Table 4 Functional characterisation of the sorbents before and after metal ion adsorption

	Wavelength (cm^{-1})						Assignment
	Before adsorption		After adsorption				
	MTR	S-MTR	MTR(Pb)	MTR(Cr)	S-MTR(Pb)	S-MTR(Cr)	
3317	3381	–	–	–	–	N–H stretching vibration of amine	
–	2114	–	–	–	–	thiol S–H stretching vibration	
1690	1683	1699	1691	1857	1700	C=O stretching vibration	
1595	1604	1602	1565	1657	1613	C=C stretching vibration for aromatic	
1205	1071	–	–	–	–	acyl C–O stretching vibration	
823–693	744–692	953–743	879–740	740–687	748–692	aromatic sp^2 C–H bend vibration	

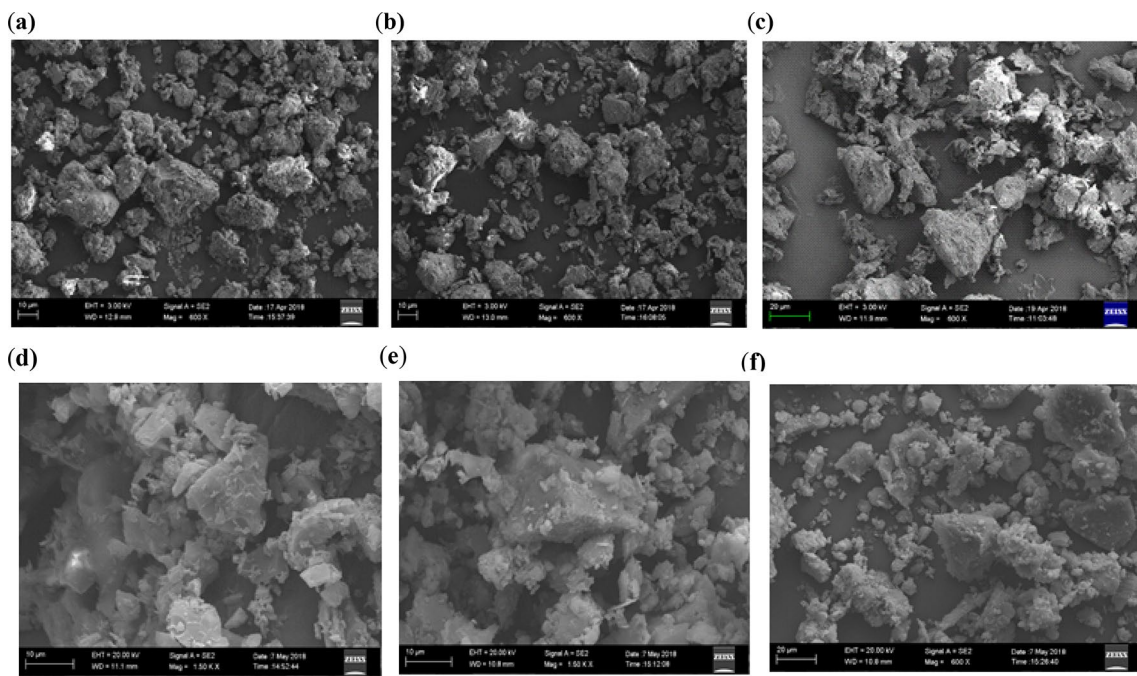


Fig. 6 Micrographs of **a** MTR, **b** MTR(Pb), and **c** MTR(Cr) **d** S-MTR, **e** S-MTR(Pb) and **f** S-MTR(Cr)

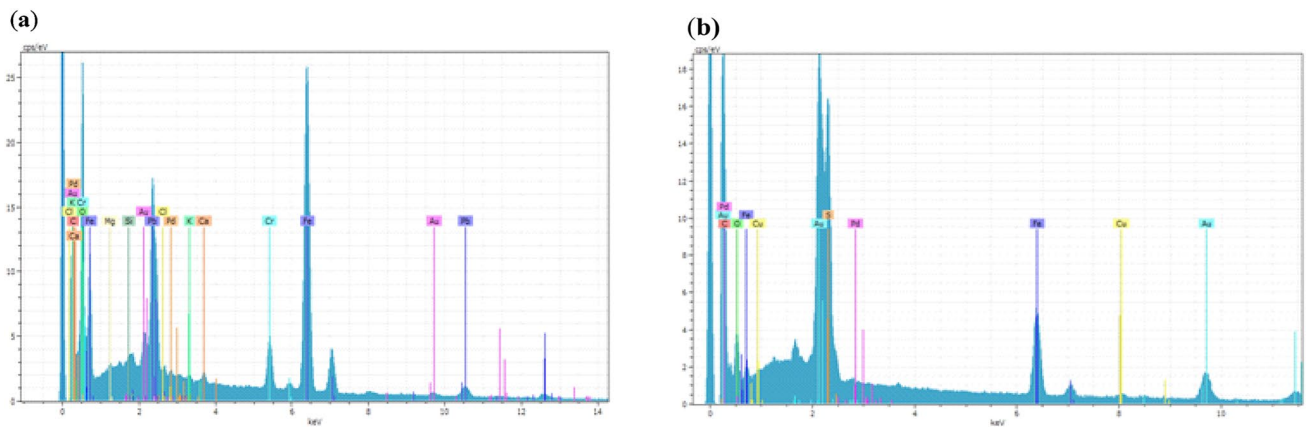


Fig. 7 Energy dispersion Spectroscopy spectra of MTR and S-MTR

content of S-MTR is lower compared to MTR due to the sulphur doping protocol.

EDX analysis of the sorbent after adsorption (Fig. S1–S2) of metal ions showed the presence of Pb(II) and Cr(VI) incorporated into the materials.

Other elements such as potassium, magnesium calcium and palladium were found on the sorbents at various concentrations, this further confirms the nature of the raw material and the phyto-chelating capacity of tannin [26].

3.3 Influence of pH, contact time, initial concentration, and temperature on adsorption capacity of the sorbents

Optimal pH determination of the adsorption of Pb(II) and Cr(VI) ions, was evaluated at a pH range of 2–8 in a batch experiment and the result is presented as shown in Fig. 9. The optimal pH for the metal ion adsorption was observed to be metal-sorbent dependent.

Maximum adsorption capacities of Pb(II) and Cr(VI) absorption by MTR was achieved at a pH 4 whereas on

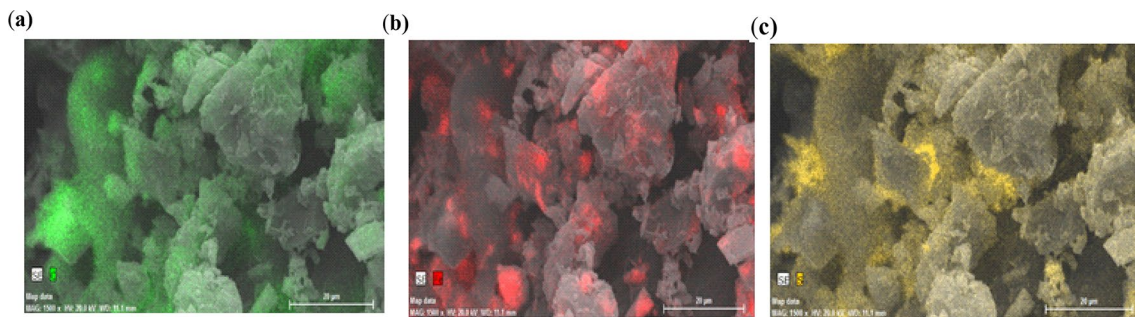


Fig. 8 Colour map micrographs of **a** TR, **b** MTR and **c** S-MTR. Key: The green mapped sites indicate carbon content of the tannin resin; red mapped sites indicate the presence of iron due to the

preparation of magnetite while the yellow mapped sites are the presence of sulphur through doping of the resin

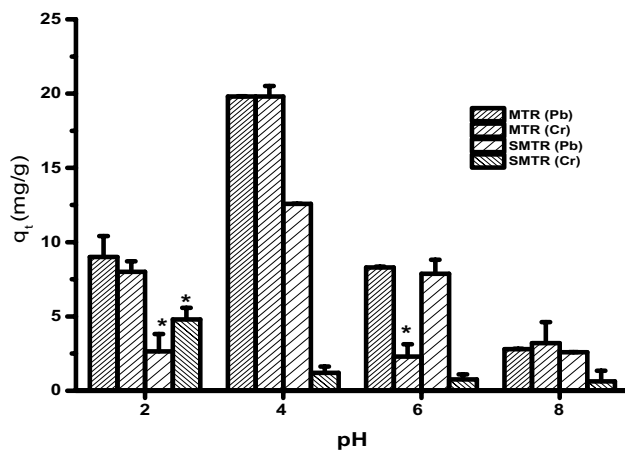


Fig. 9 Effect of pH on the metal ion adsorption capability on 0.05 g/L sorbents at 303 K. The values are expressed as mean \pm SD ($n=3$). *Significant parameters; p value < 0.05

S-MTR the optimal uptake was observed at pH values 4 and 2, respectively.

This may be attributed to the introduction of a permanent negative charge on the surface of S-MTR resulting in electrostatic attraction and ion exchange mechanism [27, 28]. Beyond pH value 4, a decrease in the adsorptions of Pb(II) and Cr(VI) on MTR was observed due to the precipitation of metal hydroxides at higher pH but not necessarily due to the repulsive effect [29, 30].

Figure 10 shows that the removal of Pb(II) and Cr(VI) from aqueous solution was found to increase with contact time; depending on the type of metal ion and nature of sorbent. An initial rapid rate of Pb(II) adsorption was observed which may be due to the affinity of MTR and S-MTR compared to Cr(VI). Consequently, the initial increase in the rate of adsorption of Pb(II) ions is possibly due to the availability of active sites with affinity and ideal pore size/volume for a specific metal ion on the surface of the adsorbents. However, the increase in the rate

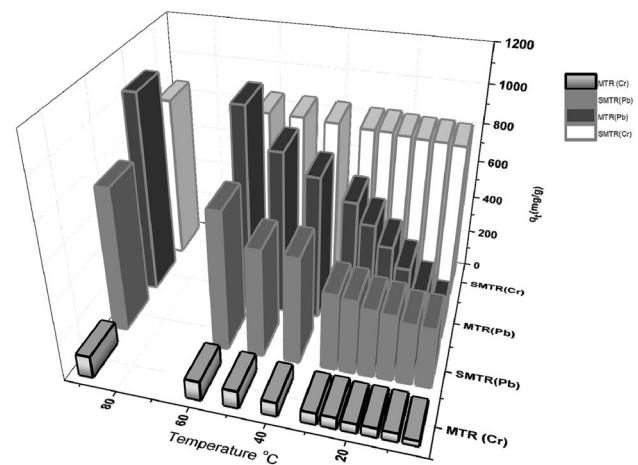


Fig. 10 Effect of contact time on metal ion adsorption capability on 0.05 g/L sorbents

of adsorption for Cr(VI) with time is not significant, due to the relatively constant adsorbate–adsorbate attractive and repulsive forces, and the lagging diffusion of the ions through the pores [31, 32].

Our investigation, revealed that the optimum contact time for adsorption for Pb(II) and Cr(VI) on MTR and S-MTR was fixed to be 70 min, respectively.

The influence of the initial concentration of the metal ions on the sorbents was evaluated by changing the concentration, while other variables were kept constant (Fig. 11). The adsorption capacity of MTR increased as Pb(II) initial concentration increased; similar adsorption capacity was reported for Pb(II) and Cr(VI) on S-MTR.

Consequently, the greater the chances of Pb(II) ion colliding with the surfaces of MTR and S-MTR at a high concentration [33]; on the other hand, the lower the probability of Cr(VI) interacting with the surfaces of both adsorbents at high concentration. Hence, the more driving force of overcoming all mass transfer resistances between the aqueous and solid phases leading to the sorption of Pb(II) on the sorbents compared to Cr(VI) [34].

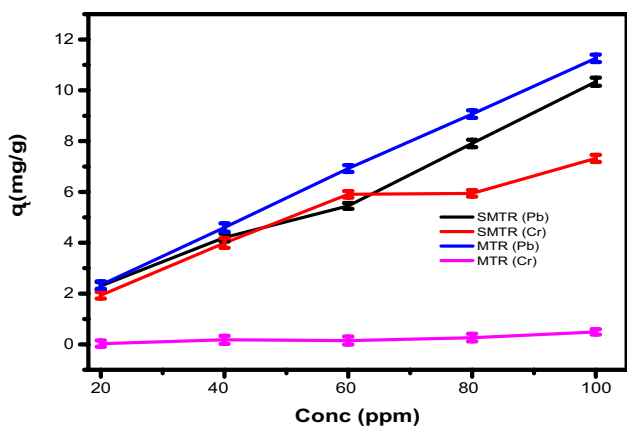


Fig. 11 Initial metal ion concentration on 0.05 g/L sorbents. The values are expressed as mean ± SD (n=3)

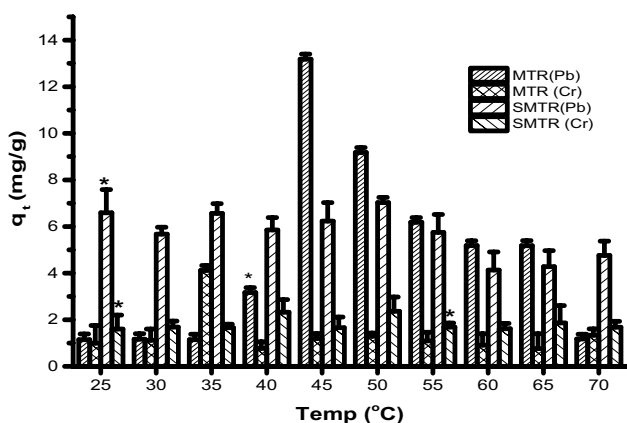


Fig. 12 Influence of temperature on metal ion adsorption capability on 0.05 g/L sorbents. The values are expressed as mean ± SD (n=3). *Significant parameters; p value < 0.05

The response of the sorbents to metal ion uptake at various temperature is presented in Fig. 12. However, temperature does not significantly affect the adsorption capacity for Pb(II) and Cr(VI) on S-MTR.

The adsorption sites on the surface of MTR are activated at relatively high temperature whereas the active sites on the surface of S-MTR are not temperature sensitive. Hence, the interaction of MTR with Pb(II) and Cr(VI) is endothermic.

3.4 Equilibrium modelling

Results from the batch equilibrium studies were used to evaluate the affinity of the adsorbents for the sorbates. Evaluation of four isotherms and their constant values were considered in the equilibrium studies to express the surface properties and affinity of the sorbents.

The Langmuir isotherm was used to express the monolayer coverage of the sorbates on the surface of the

adsorbents at a constant temperature as presented in Eq. (5):

$$\frac{C_e}{q_e} = \frac{1}{Q_{max}b} + \frac{C_e}{Q_{max}} \tag{5}$$

where q_e (mg/g), C_e (mg/L) and Q_{max} (mg/g) are the quantity of metal ion adsorbed per gram of sorbent, the concentration of an un-adsorbed metal ion in solution at equilibrium and maximum quantity of metal ion adsorbed per gram of sorbent, respectively. The affinity of the binding site is designated as b (L/mg) [35]. Plots of C_e/q_e against C_e are presented in supplementary files (Fig. S3) for the extrapolation of the Q_{max} (slope) and b (intercept). Favourabilities of metal ion adsorption on the surface of the sorbents were tested using the Langmuir isotherm dimensionless constant, R_L (separation factor) presented in Eq. (6):

$$R_L = \frac{1}{(1 + b \cdot C_o)} \tag{6}$$

Estimates of the Langmuir parameters from the interaction of Pb(II) and Cr(VI) with MTR showed good applicability of this model with correlation coefficient $R^2 = 0.8699 - 0.9747$, The Langmuir constant $b = 0.060 - 11.079$ and $R_L = 0.0009 - 0.1422$ (Table 5) as reported in the literature, that separation factor of 0 to 1 indicates favourable adsorption [36, 37].

The nature of the sorbent surface as described by Freundlich adsorption isotherm and mathematically presented in Eq. (7):

$$\text{Log}q_e = \text{Log}K_f + \frac{1}{n\text{Log}C_e} \tag{7}$$

where K_f and n are the Freundlich adsorption isotherm constant and n indicates adsorption intensity, which is related to the degree of surface heterogeneity. Both n and K_f were calculated from the slope and intercept of the plots of $\text{log}q_e$ versus $\text{log}C_e$ (Fig. S4). Studies have shown that $n \leq 1$; implies an adsorbent with homogeneous binding sites in contrast to heterogeneous surface with large n values [38].

The equilibrium data from the interactions of Pb(II) and Cr(VI) with the surface of S-MTR are better fits into the Freundlich isotherm compared to the Langmuir isotherm model. The fitness of the data into the model was determined based on the correlation coefficients, R^2 , obtained from plots (Table 5). The values of n obtained for the interactions of Pb(II) and Cr(VI) ions with surface of S-MTR were 1.373 and 1.258, respectively; suggestive of a heterogeneous binding site.

Therefore, the equilibrium adsorption data for MTR fits into the Langmuir isotherm while S-MTR mechanism is better described by the Freundlich isotherm model

Table 5 Comparison of the isotherm equations for equilibrium adsorption studies

Langmuir isotherm					Freundlich isotherm		
Sorbents	b	Q _{max} (mg/g)	R _L	R ²	n	K _f (mg/g)	R ²
MTR (Pb)	0.060	534.76	0.1422	0.9747	0.702	9600.636	0.9488
MTR (Cr)	11.079	15.10	0.0009	0.8699	1.231	23.292	0.5385
S-MTR(Pb)	1.862	813.01	0.0053	0.9432	1.373	0.003	0.9906
S-MTR(Cr)	1.525	709.22	0.0065	0.9711	1.258	0.003	0.9946
Temkin isotherm				Dubinin–Radushkevich isotherm			
Sorbents	b _T	A _T (L/mg)	R ²	Q ₀ (mg/g)	E (KJ/mol)	K _{DR} (mol ² /KJ ²)	R ²
MTR (Pb)	81.84 × 10 ⁵	3.202	0.7486	6.95	4623.34	2.34 × 10 ⁻⁸	0,8264
MTR (Cr)	78.36 × 10 ¹	0.053	0.3471	1.43	75.91	8.68 × 10 ⁻⁵	0,1607
S-MTR(Pb)	42.03 × 10 ⁴	3.173	0.8004	3.82	1769.61	1.60 × 10 ⁻⁷	0,8669
S-MTR(Cr)	34.79 × 10 ⁵	4.475	0.5908	3.90	2497.97	8.01 × 10 ⁻⁸	0,7525

governed by adsorption-complexation reactions [39]. However, the mechanism of the interactions; is adsorbent specific on a heterogeneous surface.

Also, the Dubinin–Radushkevich isotherm was evaluated using the Gaussian energy distribution as expressed in Eq. (8) [40]:

$$q_e = q_m e^{-\beta \left(RT \ln \left(1 + \frac{1}{C_e} \right) \right)^2} \quad (8)$$

where q_m (mg/g), β , R (J/mol K) and T (K); are the monolayer adsorption capacity, adsorption energy, gas constant, and absolute temperature, respectively. The plots are presented in Fig. S5 as supplementary material. Similarly, the data from the secondary ion–ion interactions on adsorption isotherm according to Temkin isotherm was considered, using the generalised form of the Temkin isotherm is expression in Eq. (9) [41]:

$$q_e = \frac{RT}{B_T} \ln A_T C_e \quad (9)$$

where A_T (L/g) and B_T are the Temkin isotherm equilibrium and binding constants. The plots are presented as supplementary file (Fig. S6) and the constants in Table 5. However, the Dubinin–Radushkevich and Temkin isotherms were not suitable models to describe the equilibrium adsorption data due to the lack of fit.

3.5 Kinetic modelling

The pseudo-first-order kinetic model, pseudo-second-order kinetic model, Elovich equation and intraparticle-diffusion equation were applied to investigate the adsorption mechanism and rate controlling steps. According to Lagergren, the pseudo-first-order rate expression is presented in Eq. (10) [42]:

$$\frac{dq_t}{dt} = k_1 (q_e - q_t) \quad (10)$$

where q (mg/g) and k_1 (min⁻¹) are the quantity of metal ion adsorbed on the surface of the sorbent at time t and the pseudo-first-order rate constant, respectively. The linear fit of the integral form of Eq. (10) shows the aptness of kinetic model in the determination of the slope (k_1) and intercept $q_{e,cal}$ (Table 6 and Fig. S7). The pseudo-second order kinetic model was applied to the kinetic data generated in this study using Eq. (11) [43]:

$$\frac{dq_t}{dt} = k_2 (q_e - q_t)^2 \quad (11)$$

where k_2 (g/mg min) is the pseudo-second-order rate constant. Using the linearised form of Eq. (11) the kinetic data were analysed at different initial metal ion concentrations. Plots of t/q versus t were used to determine the rate constant k_2 (g/mg min) and $q_{e,cal}$ (mg/g) values from the slope and intercept (Fig. S8).

The compatibility of the activated adsorption surface with a heterogeneous system was investigated by Elovich's Eq. (12) [44]:

$$\frac{dq_t}{dt} = \alpha \exp(-\beta q_t) \quad (12)$$

where α (mg/g min) and β (g/min) are the initial metal ion sorption rate, and the extent of surface coverage and chemisorption activation energy. The linear plots of qt versus $\ln t$ after applying boundary conditions and integrating gave the slope (β) and intercept (α), respectively (Fig. S9).

The theory postulated by Weber and Morris describes the particle diffusion within the adsorption system using

Table 6 The kinetics constants for the adsorption of Pb(II) and Cr(VI) on the sorbents

Sorbents	Pseudo-first-order equation			Pseudo-second-order equation		
	$k_1(\text{min}^{-1})$	$q_{e, \text{cal}}(\text{mg/g})$	R^2	$k_2(\text{g/mg min})$	$q_{e, \text{cal}}(\text{mg/g})$	R^2
MTR(Pb)	0.0843	3.5286	0.6510	3.10×10^{-4}	1111.11	0.9864
MTR(Cr)	0.0134	8.4604	0.9819	0.00019	149.25	0.9135
SMTR(Pb)	0.0235	17.4772	0.9150	4.35×10^{-5}	909.09	0.8900
SMTR(Cr)	0.0207	6.2333	0.9153	0.0016	833.33	0.9999

Sorbents	Elovich equation			Intraparticle-diffusion equation	
	$\alpha(\text{mg/g min})$	$\beta(\text{g/min})$	R^2	$K_{\text{diff}}(\text{mg/g min}^{1/2})$	R^2
MTR(Pb)	516.27	0.0060	0.4371	51.92	0.2702
MTR(Cr)	19.23	0.0334	0.9003	12.26	0.9717
SMTR(Pb)	139.03	0.0059	0.7827	8.11	0.9379
SMTR(Cr)	2.46×10^8	0.0487	0.9386	4801.50	0.7437

the intraparticle-diffusion kinetic model presented in Eq. (13) [45]:

$$q_t = k_{\text{diff}}t^{0.5} + C \tag{13}$$

where k_{diff} is the constant of intra-particle diffusion. In order, to understand the adsorption kinetic the kinetic models were applied to calculate the correlation coefficient, r^2 , from the plots (Fig. S10). The pseudo-first-order, pseudo-second-order, Elovich’s and intraparticle-diffusion kinetic models were calculated by using Eqs. (10) to (13).

The correlation coefficients, r^2 , showed that the pseudo-first order and pseudo-second-order model fits into the experimental data better for the sorption of Cr(VI) on surface of MTR and S-MTR, respectively (Figs. S7, S8 and Table 6). Hence, the interaction of Cr(VI) on MTR and S-MTR are largely physisorption and chemisorption processes, respectively; resulting in the large chemisorption extent of surface coverage for Cr(VI) is ≥ 0.0334 g/min compared to Pb(II). Conversely, the experimental data from the kinetic study of Pb(II) adsorption on MTR and S-MTR fits into pseudo-second-order and intraparticle-diffusion equation models, respectively (Supplementary files Fig. S8 and S9); hence, these are physisorption processes. The equilibrium Cr(VI) uptake capacity on the surface of MTR was found to be non-responsive with change in concentration due to the very low initial sorption rate (α) compared to the uptake of other ions by MTR and S-MTR.

3.6 Thermodynamic studies

To fully understand the nature of adsorption, the thermodynamic parameters were calculated (Table 7). The thermodynamic parameters were determined from the modified Van’t Hoff Eq. (14). The plot of $\ln K_D$ versus $1/T$ gives the enthalpy change, ΔH , (slope) and entropy change, ΔS , (intercept)

Table 7 Thermodynamics of Pb(II) and Cr(VI) adsorption on the sorbents

Sorbents	Thermodynamics parameters		
	$\Delta H(\text{KJ/mol})$	$\Delta S(\text{J/(mol-K)})$	$\Delta G(\text{KJ/mol})$
MTR(Pb)	19961.08	115.26	-14385.50
MTR(Cr)	128210.2	-408.34	249893.67
SMTR(Pb)	12588.23	-41.04	24818.76
SMTR(Cr)	-649.43	-11.51	2779.28

whereas, the change in Gibbs free energy (ΔG) is calculated from Eq. (15).

$$\ln K_D = -\frac{\Delta H}{RT} + \frac{\Delta S}{R} \tag{14}$$

$$\Delta G = \Delta H - T\Delta S \tag{15}$$

where K_D , C_s , and C_e are the equilibrium constant, concentrations of metal ions on the sorbent surface and in the liquid at equilibrium.

The Gibbs free energy (ΔG) indicates the degree of spontaneity and feasibility of the adsorption process and low values imply an energetically favourable adsorption process. The values of ΔG for the adsorption of Pb(II) onto MTR in comparison to that of S-MTR (Table 7) implies the spontaneous and feasible nature of Pb(II) sorption by MTR than S-MTR. However, adsorption of Cr(VI) on both MTR and S-MTR are not readily spontaneous and feasible due to the relatively large Gibbs free energy. The negative ΔH value of the sorption of Pb(II) on MTR confirms the releases some amount of heat during the binding Pb(II) to the surface. Conversely, the interaction of the Pb(II) and Cr(VI) on the surface of S-MTR is endothermic, indicating the feasibility of the sorption process at elevated temperature.

Entropy (ΔS) has been defined as the degree of the chaos of a system. The more negative the ΔS value, the more readily reversible and the lower the degree of randomness at the solid/liquid interface during the sorption process [46, 47].

The negative ΔG parameter of Pb(II) adsorption by MTR implies that Pb(II) in an aqueous solution of MTR treated sample was in a much more chaotic distribution compared to the relatively ordered state of solid phase at the surface of adsorbents [48].

Due to the negative ΔS values, the interaction of Pb(II) and Cr(VI) on the surface of S-MTR is a physical or reversible process, in which equilibrium is rapidly attained, and thus energy requirements are small compared to a chemical adsorption where considerable activation energy is required [47]. The activation energies for Pb adsorption onto the surface of MTR is 4623.34 kJ/mol; suggesting that Pb(II) ion are chemically adsorbed onto MTR surface; whereas, Cr(VI) is physically adsorbed. Hence, Pb(II) was strongly adsorbed onto the surface of S-MTR.

3.7 Comparison of Pb(II) and Cr(VI) adsorption with various adsorbents

The adsorption capacities of other adsorbents reported in the literature have been compared with the adsorbents in this study, as presented in Table 8. Comparatively, MTR and S-MTR have high surface adsorption capacities compared to the reference adsorbents; due to the polyphenol characteristic of the immobilized tannin resin compared to using modified biomass as an adsorbent. The difference in adsorption capacity for Pb(II) as previously reported when using tannin resin from mimosa compared to the modified tannin resins in this study is most likely due to the functionalisation and source of the tannin.

Table 8 Comparative adsorption capacities of different adsorbents

Adsorbents	Adsorbent capacity Q_{max} (mg/g)	
	Cr(VI)	Pb(II)
Activated carbon	7.0 [49]	43.9 [50]
Char of South African coal	0.3 [51]	–
Petiole of Palm Tree	–	21.8 [52]
Fibre of Palm Tree	–	23.0 [52]
Carboxymethyl cellulose-based hydrogel	6.5 [53]	–
Resin of mimosa tannin	–	13.8 [54]
Sulphur-Doped Tannin Resin (S-MTR)	709.2*	813.0*
Magnetite Tannin Resin (MTR)	15.1*	534.8*

*This study

4 Conclusion

The extraction conditions for the raw tannin were optimised by response surface modelling and the following set of conditions were obtained as ideal; a minimum mass of 6 g, pH 7, 37.5 °C, 22.5 min and 50 mL of water. Properties of the low-cost adsorbents were studied to estimate the surface area, pore volumes, and functionality of the adsorbents. In addition, the efficiencies of the modified tannin in the uptake of Pb(II) and Cr(VI) from aqueous solution were investigated and were observed to be pH-adsorbent dependent. Our study revealed that the two adsorbents optimally remove Pb(II) and Cr(VI) from aqueous solution except for uptake Pb(II) which was achieved at pH 2 on S-MTR. Further, equilibrium adsorption data obtained for the removal of ions by MTR and S-MTR showed the best fit to the Langmuir and Freundlich isotherms, respectively. Also, the sorption of Cr(VI) on MTR and S-MTR fits into the pseudo-first-order and pseudo-second-order model. However, the sorption of Pb(II) on MTR and S-MTR fits into pseudo-second-order and intraparticle-diffusion equation models, respectively. The sorption mechanism is primarily a combination of physisorption and chemisorption processes, while the thermodynamic parameters support the adsorption of Pb(II) on MTR has been feasible, spontaneous and endothermic compared to the uptake of Pb(II) and Cr(VI) by S-MTR. Comparing these modified tannins (MTR and S-MTR) with other biomass-based adsorbents in recent literature; a higher adsorption capacity of ≤ 709.2 mg/g and ≤ 813.0 mg/g for Pb(II) and Cr(VI) from aqueous solutions. Hence, MTR and S-MTR are potential alternative adsorbents for Pb(II) and Cr(VI).

Acknowledgements Our appreciation goes to the Institute of Chemical and Biotechnology, Vaal University of Technology, South Africa, for supporting the research.

Compliance with ethical standards

Conflicts of interest The authors declare that they have no conflict of interest.

References

- Hsu Y-L, Liu C-C (2010) Environmental performance evaluation and strategy management using balanced scorecard. *Environ Monit Assess* 170:599–607
- Sugita M (1978) The biological half-time of heavy metals—the existence of a third, “slowest” Component. *Int Arch Occup Environ Health* 41:25–40
- Motsi T, Rowson NA, Simmons MJH (2009) Adsorption of heavy metals from acid mine drainage by natural zeolite. *Int J Miner Process* 92:42–48

- Ahmaruzzaman M (2011) Industrial wastes as low-cost potential adsorbents for the treatment of wastewater laden with heavy metals. *Adv Colloid Interface Sci* 166:36–59
- Javadian H, Ghorbani F, Tayebi HA, Asl SMH (2015) Study of the adsorption of Cd(II) from aqueous solution using zeolite-based geopolymer, synthesized from coal fly ash; kinetic, isotherm and thermodynamic studies. *Arab J Chem* 8:837–849
- Ling A, Jiawei H, Yiyang W, Jingjing Zhan, Chaoliang W (2016) Aerosol-assisted in situ synthesis of iron-carbon composites for the synergistic adsorption and reduction of Cr(VI). *RSC Adv* 6:56108–56115
- Pradhan D, Sukla LB (2018) Bioreduction of hexavalent chromium using microalgae. Springer, Berlin, pp 65–73
- Abas SNA, Ismail MHS, Kamal ML, Izhar S (2013) Process, adsorption low-, of heavy metals by review”, cost adsorbent: a journal. *World Appl Sci* 28:1518–1530
- Abdel OE, Reiad NA, ElShafei MM, Abdel Salam OE, Reiad NA, ElShafei NM (2011) A study of the removal characteristics of heavy metals from wastewater by low-cost adsorbents. *J Adv Res* 2:297–303
- Lee CG, Song MK, Ryu JC, Park C, Choi JW, Lee SH (2016) Application of carbon foam for heavy metal removal from industrial plating wastewater and toxicity evaluation of the adsorbent. *Chemosphere* 153:1–9
- Pradhan D, Sukla LB, Mishra BB, Devi N (2019) Biosorption for removal of hexavalent chromium using microalgae *Scenedesmus* sp. *J Clean Prod* 209:617–629
- Yamaguchi H, Higashida R, Higuchi M, Sakata I (1992) Adsorption mechanism of heavy-metal ion by microspherical tannin resin. *J Appl Polym Sci* 45:1463–1472
- Sakaguchi T, Nakajima A (1986) Recovery of Uranium by Immobilized Polyhydroxyanthraquinone. *Sep Sci Technol* 21:519–534
- Mueller Ferdinand von (1884) Select extra-tropical plants readily eligible for industrial culture or... Ferdinand von Mueller
- Okoli BJ, Shilowa P, Anyanwu G, Modise JS (2018) Removal of Pb²⁺ from water by synthesized tannin resins from invasive South African Trees. *Water (Switzerland)* 10:648
- Montgomery DC (2001) Design and analysis of experiments, 5th edn. Wiley, New York, pp 14–20
- Myers RH, Montgomery DC (2002) Process and product optimization using designed experiments, 2nd edn. Wiley, New York, pp 1–25
- Okoli CP, Naidoo EB, Ofomaja AE (2018) Role of synthesis process variables on magnetic functionality, thermal stability, and tetracycline adsorption by magnetic starch nanocomposite. *Environ Nanotechnol Monit Manag* 9:141–153
- Sieniawska E, Baj T (2017) Tannins Pharmacogn Fundam Appl Strateg. Elsevier, Amsterdam, pp 199–232
- Sing K (2001) The use of nitrogen adsorption for the characterization of porous materials. 188:3–9
- Ünlü N, Ersoz M (2006) Adsorption characteristics of heavy metal ions onto a low cost biopolymeric sorbent from aqueous solutions. *J Hazard Mater* 136:272–280
- Xia Y, Mokaya R, Walker GS, Zhu Y (2011) Superior CO₂ adsorption capacity on N-doped, high-surface-area, microporous carbons templated from zeolite. *Adv Energy Mater* 1:678–683
- Svatos GF, Curran C, Quagliano JV (1955) Infrared absorption spectra of inorganic coordination complexes. V. The N–H stretching vibration in coordination compounds. *J Am Chem Soc* 77:6159–6163
- Rao C, Kastur R, Exkataraghavav T (1964) Contribution to the infrared spectra of organosulphur compounds. *Can J Chem* 42:36–42
- Miller BJ, Howard DL, Lane JR, Kjaergaard HG, Dunn ME, Vaida V (2009) SH-Stretching vibrational spectra of ethanethiol and *tert*-Butylthiol. *J Phys Chem A* 113:7576–7583
- Karamać M (2009) Chelation of Cu(II), Zn(II), and Fe(II) by tannin constituents of selected edible nuts. *Int J Mol Sci* 10:5485–5497
- Zhang Y-J, Ou J-L, Duan Z-K, Xing Z-J, Wang Y (2015) Adsorption of Cr(VI) on bamboo bark-based activated carbon in the absence and presence of humic acid. *Colloids Surfaces A Physicochem Eng Asp* 481:108–116
- Tavengwa NT, Cukrowska E, Chimuka L (2016) Application of raw and biocharred *Moringa oleifera* seed powder for the removal of nitrobenzene from aqueous solutions. *Desalin Water Treat* 57:25551–25560
- Dong L, Zhu Z, Ma H, Qiu Y, Zhao J (2010) Simultaneous adsorption of lead and cadmium on MnO₂-loaded resin. *J Environ Sci* 22:225–229
- Kiran I, Ozcan A (2006) Equilibrium and kinetics of biosorption of lead (II) from aqueous solutions by *Cephalosporium aphidicola*. *Sep Purif Technol* 47:105–112
- Karthikeyan T, Rajgopal S, Miranda LR (2005) Chromium(VI) adsorption from aqueous solution by *Hevea brasiliensis* sawdust activated carbon. *J Hazard Mater* 124:192–199
- Danish M, Hashim R, Rafatullah M, Sulaiman O, Ahmad AA (2011) Adsorption of Pb(II) Ions from Aqueous Solutions by Date Bead Carbon Activated with ZnCl₂. *Clean—Soil, Air, Water* 39:392–399
- Anirudhan TS, Suchithra PS (2010) Synthesis and characterization of iron(III)-coordinated amine-modified poly(glycidylmethacrylate)-grafted densified cellulose and its applicability in defluoridation from industry effluents. *Ind Eng Chem Res* 49:12254–12262
- Jung C, Heo J, Han J, Her N, Lee SJ, Oh J, Ryu J, Yoon Y (2013) Hexavalent chromium removal by various adsorbents: powdered activated carbon, chitosan, and single/multi-walled carbon nanotubes. *Sep Purif Technol* 106:63–71
- Langmuir I (1918) The adsorption of gases on plane surfaces of glass, mica and platinum. *J Am Chem Soc* 40:1361–1403
- Ćurko J, Matošić M, Crnek V, Stulić V, Mijatović I (2016) Adsorption characteristics of different adsorbents and Iron(III) salt for removing As(V) from water. *Food Technol Biotechnol* 54:250–255
- Sviloviæ S, Rušić D (2008) Thermodynamics and adsorption isotherms of copper ions removal from solutions using synthetic zeolite X. *Chem Biochem Eng Q* 22:299–305
- Chen H, Zhao Y, Wang A (2007) Removal of Cu (II) from aqueous solution by adsorption onto acid-activated palygorskite. *J Hazard Mater* 149:346–354
- Bulut Y, Tez Z (2007) Removal of heavy metals from aqueous solution by sawdust adsorption. *J Environ Sci (China)* 19:160–166
- Karamać M (2007) Fe(II), Cu(II) and Zn(II) chelating activity of buckwheat and buckwheat tannin groats tannin fractions. *Polish J Food Nutr Sci* 57:357–362
- Ho YS, Ng JCY, McKay G (2001) Removal of lead(II) from effluents by sorption on peat using second-order kinetics. *Sep Sci Technol* 36:241–261
- Lagergren S (1898) About the theory of so-called adsorption of soluble substances, 24th ed
- Binaeian E, Seghatoleslami N, Chaichi MJ (2016) Synthesis of oak gall tannin-immobilized hexagonal mesoporous silicate (OGT-HMS) as a new super adsorbent for the removal of anionic dye from aqueous solution. *Desalin Water Treat* 57:8420–8436
- Cheung CW, Porter JF, McKay G (2001) Sorption kinetic analysis for the removal of cadmium ions from effluents using bone char. *Water Res* 35:605–612

45. Morris WJW, Morris JC (1963) Kinetics of adsorption on carbon from solution. *J Sanit Eng Div* 89:31–60
46. Sheikhsosseini A, Shariatmadari H, Shirvani M, Zvomuya F (2012) Kinetics and thermodynamics of nickel sorption to calcium-palygorskite and calcium-sepiolite : a batch study Kinetics and thermodynamics of nickel sorption to calcium- palygorskite and calcium-sepiolite : a batch study. *Geoderma* 217:1–28
47. Boparai HK, Joseph M, O'Carroll DM (2011) Kinetics and thermodynamics of cadmium ion removal by adsorption onto nano zerovalent iron particles. *J Hazard Mater* 186:458–465
48. Sdiri A, Higashi T, Hatta T, Jamoussi F, Tase N (2011) Evaluating the adsorptive capacity of montmorillonitic and calcareous clays on the removal of several heavy metals in aqueous systems. *Chem Eng J* 172:37–46
49. Gholipour M, Rafsanjani HH, Goharrizi AS (2011) Optimization and modeling of hexavalent chromium removal from aqueous solution via adsorption on multiwalled carbon nanotubes. *J Eng Appl Sci* 3:880–886
50. Acharya J, Sahu JN, Mohanty CR, Meikap BC (2009) Removal of lead (II) from wastewater by activated carbon developed from Tamarind wood by zinc chloride activation. *Chem Eng J* 149:249–262
51. Di Natale F, Lancia A, Molino A, Musmarra D (2007) Removal of chromium ions from aqueous solutions by adsorption on activated carbon and char. *J Hazard Mater* 145:381–390
52. Hikmat NA, Qassim BB, Khethi MT (2014) Thermodynamic and kinetic studies of lead adsorption from aqueous solution onto petiole and fiber of palm tree. 4:116–124
53. Chen S, Jin L, Chen X (2011) Procedia engineering the effect and prediction of temperature on adsorption capability of coal/CH₄. *Procedia Eng* 26:126–131
54. Luzardo FHM, Velasco FG, Correia IKS, Silva PMS, Salay LC (2017) Removal of lead ions from water using a resin of mimosa tannin and carbon nanotubes. *Environ Technol Innov* 7:219–228

Publisher's Note Springer Nature remains neutral with regard to jurisdictional claims in published maps and institutional affiliations.